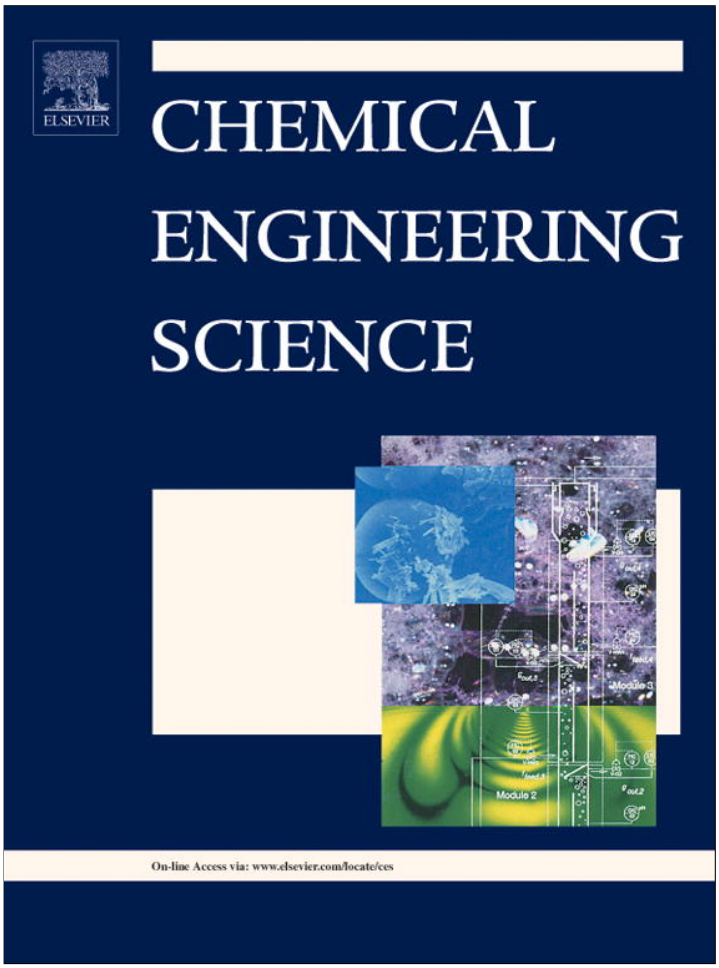

(This is a sample cover image for this issue. The actual cover is not yet available at this time.)

Chemical Engineering Science 81 (2012) 84–90

Contents lists available at SciVerse ScienceDirect

Chemical Engineering Science

journal homepage: www.elsevier.com/locate/ces

Analysis of $W_1/O/W_2$ double emulsions with CLSM: Statistical image processing for droplet size distribution

Sandy Schuster [a], Richard Bernewitz [a,b], Gisela Guthausen [b,*], Jascha Zapp [c], Alexandra M. Greiner [d], Karsten Köhler [a], Heike P. Schuchmann [a]

[a] Institute of Process Engineering in Life Science, Section of Food Engineering, KIT, 76131 Karlsruhe, Germany
[b] SRG 10-2, Institute for Mechanical Engineering and Mechanics, KIT, 76131 Karlsruhe, Germany
[c] Computer Assisted Clinical Medicine, Heidelberg University, 68167 Mannheim, Germany
[d] Zoological Institute, Department of Cell- and Neurobiology, KIT, 76131 Karlsruhe, Germany

HIGHLIGHTS

- Imaging of (double-) emulsions via confocal laser scanning microscope (CLSM).
- Influence of systematic errors of CLSM, and their corrections.
- Importance of the number of analysed objects in the statistical image processing.
- Simultaneous measuring of different phases of double emulsions.

ARTICLE INFO

Article history:
Received 26 October 2011
Received in revised form
26 March 2012
Accepted 27 June 2012
Available online 7 July 2012

Keywords:
Emulsion
Food processing
Imaging
Microstructure
Confocal laser scanning microscope (CLSM)
Droplet size distribution by statistical image analysis

ABSTRACT

Droplet size distribution is an important measure in processing of (food) emulsions, due to its influence on relevant product characteristics as e.g. taste, mouth feel and texture. Analysis of droplet sizes in more complex structures like double emulsions is currently a challenge for common measuring techniques (e.g. laser diffraction). Apart from nuclear magnetic resonance, optical microscopy shows potential to measure the encapsulated droplets of (double-) emulsions. Statistical image processing can be applied to get particle or droplet size distributions from confocal laser scanning microscope (CLSM) images. CLSM is well suited for the characterisation of emulsion systems and has already been applied to single emulsions. In this study, it is combined with statistical image processing with the aim to obtain droplet size distributions of droplets, dispersed in droplets (double-emulsions). The question is addressed whether an accurate droplet size distribution can be extracted from a set of images in spite of the systematic errors of the measurement method itself. Algorithms for error correction and for estimation of a statistically relevant number of objects are presented. The results from image data processing are compared with data from other measuring techniques on single and double emulsions as well as glass particle suspensions. Corrected CLSM data are in good agreement with measured values from the laser diffraction on single emulsions and glass particle suspensions. A simultaneous representation of the inner and outer phase of a double emulsion is possible.

1. Introduction

Due to increasing demands on emulsion-based products, pharmaceutical and cosmetic industry require the development of new complex materials like double emulsions (Muschiolik, 2007). Objectives as e.g. fat reduction and encapsulation of active ingredients (Benichou et al., 2004; McClements et al., 2009) are addressed by double emulsions. They can also be used as micro-reactors (Landfester, 2009) for production of hybrid nano-particles of target size and inner structure. With respect to fat reduction and encapsulation of hydrophilic (bio-) actives for life science applications, water-in-oil-in-water ($W_1/O/W_2$)-emulsions are of special importance. For the controlled production, the droplet size distributions (DSD) of the inner and outer disperse phase as well as the volume fractions are essential to be known. Structure-related product properties and stability are important especially with respect to industrial applications and are controlled by these measures. Common methods for the characterisation of simple emulsions (e.g. laser diffraction, dynamic light scattering, ultrasonic attenuation) are limited or not explored regarding the

* Corresponding author. Tel.: +49 0 721 60848058; fax: +49 0 721 60844953.
E-mail address: gisela.guthausen@kit.edu (G. Guthausen).

0009-2509/$ - see front matter © 2012 Elsevier Ltd. All rights reserved.
http://dx.doi.org/10.1016/j.ces.2012.06.059

characterisation of double emulsions. Apart from these scattering methods, imaging methods can be applied. Common light microscopes do not provide sufficient differentiation between the phases and is a projection method. Regarding small droplet diameters ($d \leq 1$ μm), scattered light causes additional noise which limits the effective resolution. Confocal laser scanning microscopy (CLSM) is capable of creating high contrasts between the phases, using appropriate fluorescence markers. Another important advantage is the pinhole (aperture). A pinhole with adjustable diameter allows blinding out the out-of-focus light, leading to a slice selection with adjustable thickness: The smaller the pinhole the sharper and thinner the optical slice (Pawley, 1995). Additionally, it minimises noise caused by scattered light.

For a detailed insight into samples, CLSM allows an in-situ observation of processes. For example, the spatial distribution of encapsulated drugs in double emulsions can be visualised (Mao et al., 2007). CLSM is well suited for the evaluation of microstructures of simple emulsions (Blonk and Vanaalst, 1993; van Dalen, 2002). A dynamic view illustrating structural changes can be used for developing new foods (Blonk and Vanaalst, 1993). It is also used as a characterisation tool for different types of complex micro-particles (Lamprecht et al., 2000) inter alia double emulsions. Comparing DSDs from nuclear magnetic resonance (NMR) and CLSM, it was shown that the precision of the CLSM method strongly depends on the number of counted droplets (van Duynhoven et al., 2002).

Depending on the application, the advantages of CLSM can turn into sources of systematic errors. Two of them are discussed with respect to the determination of DSDs: due to the optical slicing it can no longer be assumed that the droplets are detected at their centre, i.e. at the largest diameter, or even imaged at all. The probability of especially small droplets positioned above or below the focal plane without being detected is larger than the probability for relatively large droplets (Gegner et al., 2004; Skorobogat and Podobeda, 1975; van Dalen, 2002).

The second source of error is that droplets are cut by the image field of view, leading to a statistically less relevant number of analysed droplets and additionally to a reduced diameter for those droplets which are partially imaged (van Dalen, 2002).

In this article, statistical image processing of CLSM images regarding the determination of the DSD of (double-) emulsions is discussed. The effects of slicing and limited image field of view are analysed with respect to the question whether an accurate droplet size distribution can be extracted from a set of CLSM images. Algorithms are presented, and the results from image processing are compared with data from other measuring techniques on single and double emulsions.

2. Methods

2.1. Preparation of double emulsions

All $W_1/O/W_2$ double emulsions were prepared in a two-step procedure. In the first step an aqueous phase (W_1) was dispersed into an oil phase (O), yielding the inner W_1/O emulsion. In a second step, the inner W_1/O emulsion was dispersed into another aqueous phase (W_2).

As oil soluble emulsifier, PGPR 90 (GRINDSTED® PGPR 90 Kosher, Danisco A/S, E476, Material No. 033624, Grindsted, Denmark) was dissolved with a concentration of 10 wt% in pure vegetable oil (Floreal Haagen GmbH, Saarbrücken, Germany) while heating up to 40 °C and stirring with a magnetic stirrer. In the inner aqueous phase (demineralised water), 0.5 wt% gelatine (RUF Lebensmittelwerk KG, Quakenburg, Germany) were dissolved also by heating up to 40 °C while stirred on a separated magnetic stirrer. Gelatine causes an improved stability against coalescence of the aqueous phase (W_1), which was slowly added to the oil phase (O) while stirring with a propeller stirrer (400 rpm for 2 min). The obtained W_1/O emulsion premix, with a disperse phase ratio of 60%, was emulsified for 5 min with a tooth rim dispersing machine at 15,000 rpm (MagicLAB® Modul UTL-double-breasted, IKA®-Werke GmbH & Co KG, Staufen, Germany). To ensure a complete gelation of the water phase (W_1), the W_1/O emulsion was cooled at 4 °C for 1 h. To reach the desired disperse phase ratio of 30%, the W_1/O emulsion was subsequently diluted with vegetable oil, containing 5% PGPR 90. These emulsions were characterised by laser diffraction with respect to their DSD.

The outer aqueous phase of the double emulsion (W_2) was prepared with 2 wt% of the water soluble emulsifier LUTENSOL TO 10 (C_{13} Oxo Alcohol Ethoxylates, iso-$C_{13}H_{27}O(CH_2CH_2O)_{10}H$, Art.-Nr. 50070867, BASF AG, Ludwigshafen, Germany) by stirring with a magnetic stirrer. Subsequently a second premix was produced by adding the W_1/O emulsion 1:1 slowly to the prepared aqueous phase (W_2) while stirring with a spoon. This premix of the double emulsion was emulsified with a colloid mill (MagicLAB® Modul MK, IKA®-Werke GmbH & Co KG, Staufen, Germany) for 5 min at 7000 rpm and a radial gap of 0.159 mm.

For a separate analysis of each phase with CLSM, different fluorescent dyes were added to the W_1- and O-phase. In the oil phase 5 mg/l Nile Red (Acros Organics–Thermo Fisher Scientific, CAS: 415711000, Geel, Belgium) were solved. 10 mg/l Fluorescein Sodium (Carl Roth, CAS: 518478, Karlsruhe, Germany) were added to the aqueous phase.

2.2. Image acquisition with CLSM

The microscope LSM 510 META (Carl Zeiss Microscope Systems, Jena, Germany) was used for imaging the (double) emulsions with differently dyed phases. The fluorescence molecules were excited with an Argon-laser (488 nm) for Fluorescein–Sodium in the water phase (maximum absorption/emission approx. 490/514 nm) and an Argon/Krypton-laser (561 nm) for Nile Red in the oil phase (maximum absorption/emission: 550/590 nm). The optical magnification was achieved by a plan apochromat 63× (NA 1.4) objective using Immersol™ 518F (Zeiss, Oberkochen, Germany) as an immersion medium. The emitted light from Nile Red was limited by a band-elimination filter in a range 572–615 nm. Another band-elimination filter limited the emitted light from Fluorescein–Sodium in a range 505–530 nm. As only the dye molecules of the different phases are visualised by CLSM, foreign phases as air bubbles do not influence the positive images. The pinhole was adjusted between 50 μm and 100 μm, depending on the sample. The smaller the pinhole the sharper and thinner the optical slice (Pawley, 1995), which normally amounts to less than 1 μm. The pinhole is therefore crucial for the confocality, which is defined by the congruence of exposure level and observation level. The in-slice optical resolution of the quadratic images amounted to 1024 pixels × 1024 pixels with an image size of 142.9 μm × 142.9 μm, i.e. an isotropic resolution of 0.1396 μm/pixel. The heat input due to the light source leads to a fast movement of droplets, so that the exposure time had to be decreased. An exposure time between 1.28 and 3.2 μs per pixel was chosen. The laser power and detector sensitivity are optimised for each sample as they strongly depend on the sample properties. The images are acquired in the Zeiss LSM 510 operating software (V 4.2 SP1).

2.3. Image data processing with ImageJ

For analysis of the CLSM image sections, the open source software ImageJ (V 1.43 u, freeware, http://rsbweb.nih.gov/ij/)

was used. The first step was the conversion of the red channel into a binary image. The automatic threshold function "*make binary*" was applied for creating black-white images. After the noise reduction with the function "*despeckle*", a border was constructed around black droplets (W_1) on the phase transition between the oil and outer water phase. The oil film around W_1 droplets on the border of oil droplets is thin and fluorescent emission is low. Due to thresholding, it might happen that this thin oil film is no longer visible in the CLSM binary image, so that the boundary between inner and outer water phase must be reconstructed. This was realised by the "watershed" function. Subsequently black objects with specified circularity between 0.7 and 1 were extracted. The circularity C_o is proportional to the ratio of projected area A of a detected object to the square of its circumference U: $C_o=4\pi A/U^2$. C_o can take values between 0 (elongated polygon objects) and 1 (perfectly spherical objects). Subsequently, droplets or particles can be excluded which show a bad production- and image processing-related shape. The function "*watershed*" was also used to separate fully filled black droplets which are close to each other. All extracted image objects were analysed with subsequent calculation of volume-weighted DSD. The minimum class width is given by the digital resolution of the CLSM. The effectively used class width in the DSD depends on the emulsion and the corrections described in the following section.

2.4. Correction of the slice error (Scheil–Saltykov)

The slice error considers on the one hand the lower probability of small droplets to be detected in the focal slice (Fig. 1(a)). If the slice thickness is small compared to the sample thickness, a certain probability exists that droplets especially with small diameters are not detected at all. On the other hand, the droplets are not necessarily intersected at the centre. The diameter of a droplet's intersection does therefore not necessarily correspond to the "real" diameter of a given droplet (van Dalen, 2002; van Duynhoven et al., 2002; Wicksell, 1925). An optical circle diameter is related to many droplet diameters (Fig. 1(b)). Vice-versa, the variety of slicing possibilities of a given droplet results in different optical circle diameters.

The first effect shifts the DSD towards a larger median, whereas the second effect reduces the effective diameters of the larger droplets in the DSD. The slice error therefore results in an apparent narrowing of the DSD. Different mathematical error correction algorithms are known in literature. Some of them assume a specific form of the size distribution; these approaches are not considered here. Based on the model-free stereology, Wicksell assumed a continuous distribution (Wicksell, 1925), whereas Goldsmith (Goldsmith, 1967), Scheil and Saltykov (Gegner et al., 2004) as well as Cruz-Orive (Cruz-Orive, 1976, 1983) used discrete distributions in the algorithms for correcting the size distribution from images. In these approaches, the distribution and the sizes are classified. For both, the corrected distribution and the distribution obtained from the images, the class widths and the number of classes are chosen identical. The difference between the latter approaches can be found in the definition of the class size median, which can approximately be neglected in the case of a large distribution width compared the class size width. The differences of the methods were found to be rather small in a numerical comparison (Reverter et al., 1993).

The mathematical correction method according to Scheil–Saltykov (Gegner et al., 2004) was implemented in Matlab® (V 2010a): consider a system of randomly arranged spheres of different diameters in a unit volume. Slicing leads to different optical circle diameters of a given sphere. When evaluating a statistically sufficiently large number of intersection circles, it can be assumed that the largest droplet diameter in the sample is given by the largest optical circle diameter. On basis of this assumption, the DSD is calculated regressively, starting from the largest circle diameter. The entity is divided into a number N_s of size classes with width Δ. An optical circle diameter of size class i can be due to a "real" droplet diameter between the maximum diameter of class $j=N_s-1$ and its own optical circle diameter class $j=l$. Vice versa, a droplet in class j can provide an optical circle diameter in the class $i=0$ up to its own class $i=j$ (Fig. 1(b)). With the Scheil–Saltykov algorithm, the incorrect size distribution of circle diameters will be redirected (Fig. 1). Detailed explanations can be found in (Gegner et al., 2004; Sommer, 1979).

2.5. Correction of optical section error

In CLSM, optical sections are recorded (Fig. 2). Their size is limited by the optical magnification. Thereby droplets are cut by the frame of the quadratic optical section (also named mask or field of view); their volume cannot be calculated on basis of the chord. The probability to be cut by the optical frame increases with increasing ratio of droplet size to a given length of edge. This error would attenuate the contribution of larger droplets to the DSD. The same effect would be achieved, if the cut droplets would be excluded from their analysis (Sommer, 1995; van Dalen, 2002). A methodical correction can be done in analogy to the maximum Feret diameter for consideration of all droplets. The maximum Feret diameter is the largest distance between two points on the boundary of an object. In the present context, it is understood as the largest chord. In the case of droplets with more than half the size within the optical frame, the largest chord corresponds to the diameter. This correction is not exact, because droplets that are

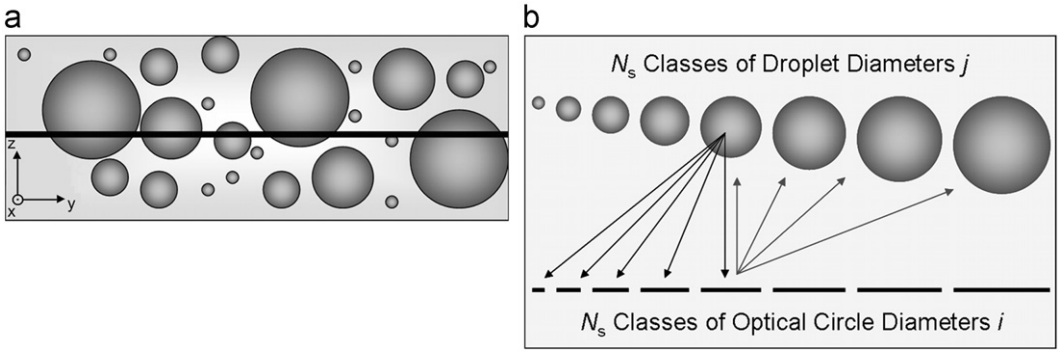

Fig. 1. Schematic illustration of the slice error: (a) the probability for a droplet to be detected in the focal plane increases with its droplet size. Especially small droplets can be above or below the focal plane without being detected. Detected droplets are optically cut through their centre only rarely. (b) Relation between optical circle diameter and "true" droplet diameters. The variety of slicing possibilities of a given droplet results in different optical circle diameters.

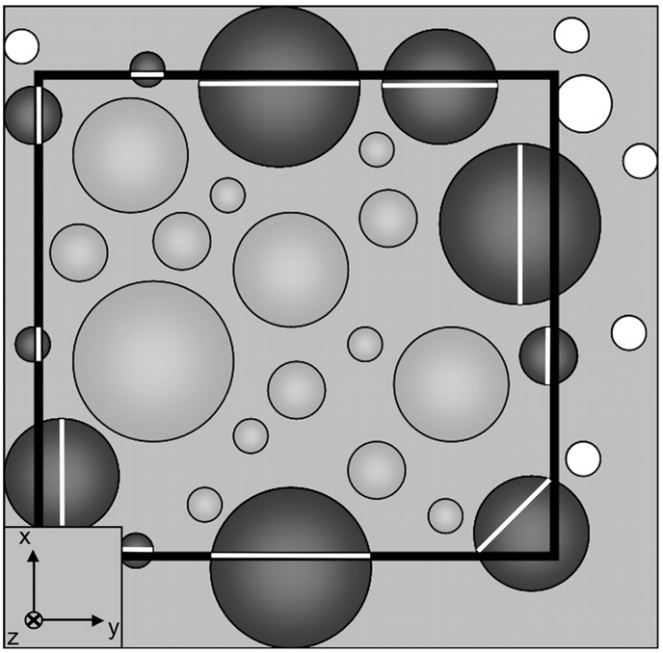

Fig. 2. Scheme of the optical section error: the optical section error increases with increasing ratio of the droplet size to the length of an optical section edge. To reduce the statistical inaccuracy due to the elimination of cut droplets, the maximum Feret diameter (indicated by the white bars) was used, considering all droplets.

located with their centre outside the selection frame will still provide an error. This error is, however, reduced compared to the error made when completely excluding the cut droplets.

3. Results and discussion

3.1. CLSM on Emulsions: influence of dyeing

In Fig. 3 CLSM images of a single W/O-emulsion are shown. Principally, each phase of an emulsion can be dyed: Fig. 3(a) shows the emulsion with the quasi-continuous oil phase dyed by Nile Red, whereas Fig. 3(b) shows the CLSM image of the emulsion with dyed dispersed water phase by addition of Fluorescein–Sodium. By comparing the results of both images, it is found that dyeing of the quasi-continuous phase leads to a more reliable image. Droplets which are close to the focal plane contribute to an incorrect count. Dyeing the quasi-continuous phase, out-of-focus light can be reduced (van Dalen, 2002). Moreover, out-of-focus light makes rendering difficult due to diminished contrast. The uncorrected DSD, however, suffers from the systematic errors mentioned above, apart from the statistical uncertainty due to the limited signal-to-noise ratio. DSDs obtained from the CLSM images via statistical image processing can be corrected by mathematical treatments to compensate the error of image slicing (van Dalen, 2002).

3.2. Influence of individual errors and their corrections

In order to correct the DSD with respect to the slicing and the optical section errors, the order of magnitude of these systematic errors has to be explored. To illustrate and quantify the errors and the associated correction procedures, a model system with spherical glass particles in stained vegetable oil was used (Fig. 4(a) inset). First, CLSM images showed that in addition to spherical glass particles, fragments were present. To rule out this additional error, a minimum circularity C_o of 0.75 was applied to exclude fragments. The optical section error is relatively small in this case; the correction has a minimal effect on the volume-specific cumulative distribution Q_3. The reason is likely to be seen in the high circularity, since large edge-cut particles were not analysed due to $C_o=0.75$. The ratio of the average particle size to the dimension of the edge length of the image amounts to about 0.073. This value is well below 1, resulting in a very small optical section error.

In contrast, the correction of the slice error according to Scheil–Saltykov (Gegner et al., 2004) shows a more pronounced shift in Q_3 to the direction of larger particles in the coarse material and only a minimal shift towards smaller particles in the fine material (Fig. 4(a)).

To avoid a misinterpretation due to the strong influence of the diameter in the cumulative volume related distribution function Q_3, a number related distribution Q_0, respectively its density q_0 is calculated (Fig. 5). Both are related via the following equations:

$$q_3(\overline{d}_n)=\frac{Q_3(d_{n+1})-Q_3(d_n)}{d_{n+1}-d_n} \tag{1}$$

$$q_0(\overline{d}_n)=\frac{\overline{d}_n^{-3}q_3(\overline{d}_n)}{\sum_{k=1}^{N}\overline{d}_k^{-3}q_3(\overline{d}_k)} \tag{2}$$

with N, the number of size classes and their interval $[d_n, d_{n+1}]$ with centre $\overline{d}_n$.

In Fig. 5, the two corrections are compared to the original data. As expected, the methodical correction of the optical section error shifts the q_0 distribution to larger particles (Fig. 5(a)). The reason is the above mentioned dependence of the error on the ratio of particle size and edge length of the optical section frame. Large particles tend to be more often cut. However, this error does not strongly affect the distribution; therefore this correction can probably be neglected in the case of sufficiently large numbers of analysed objects. The situation is different for the slice error and its mathematical correction according to Scheil–Saltykov (Fig. 5(b)). It causes a significant redistribution of particle sizes towards a broader DSD, and thus counteracts the low probability for the detection of smaller particles.

In order to get an estimate for the accuracy of the statistical image analysis and the correction methods, a comparison with other methods for the determination of the DSD was performed. In the case of glass particles in oil, two established methods were used. Their results are compared to the CLSM analysis in Fig. 4(b). The median of the distribution is shifted to slightly larger diameters in the case of CLSM; the distribution widths are similar for all three methods. A good agreement is found for $d_{90,3}$ and $d_{10,3}$ for either laser diffraction or the Coulter Counter principle, respectively. Thereby, the quantities $d_{x,3}$ are the characteristic numbers of the corresponding volume related distribution, indicated by the subscript 3. $d_{50,3}$, for example, is the median, $d_{10,3}$ indicates the 10% quantile. Comparing the deviation between the two established methods with the deviation of the CLSM, it can be concluded that it is in an acceptable range.

3.3. Statistical influences of the number of analysed objects

A statistically relevant image analysis has to consider a minimum number of objects. In the case of a known number related distribution Q_0 and a given tolerated relative error f_{rel}, the minimum number of droplets can be calculated according to

$$n=\frac{t^2}{f_{rel}^2}\left(\frac{1}{Q_0}-1\right) \tag{3}$$

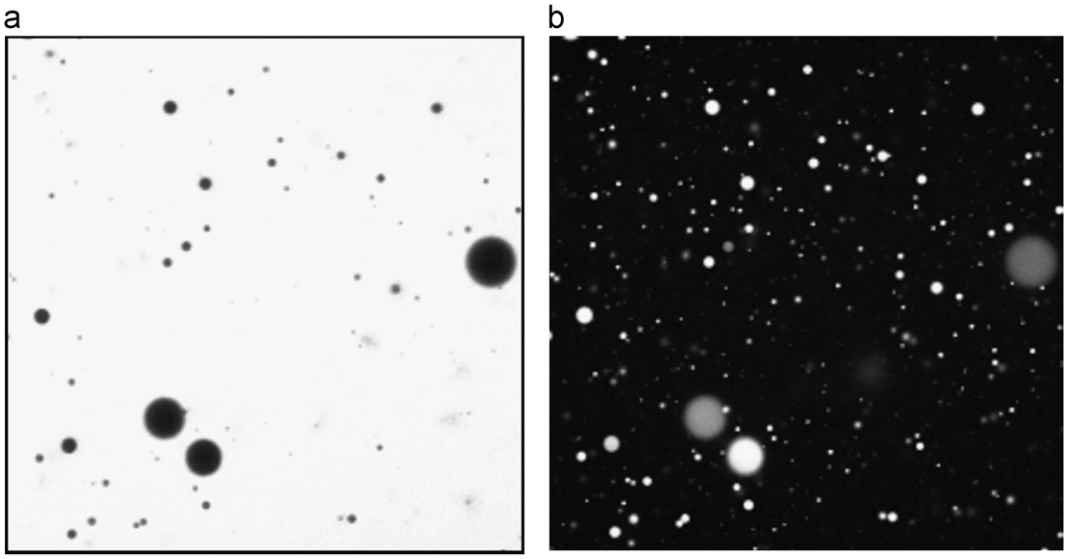

Fig. 3. CLSM images of a W/O emulsion: due to different dyeing the images are not geometrically congruent to each other. (a) Nile Red in the oil phase, (b) Fluorescein–Sodium in the water phase. Dyeing of the continuous phase results in an additional reduction of out-of-focus light. In both cases the field of view amounts to 142.9 μm × 142.9 μm.

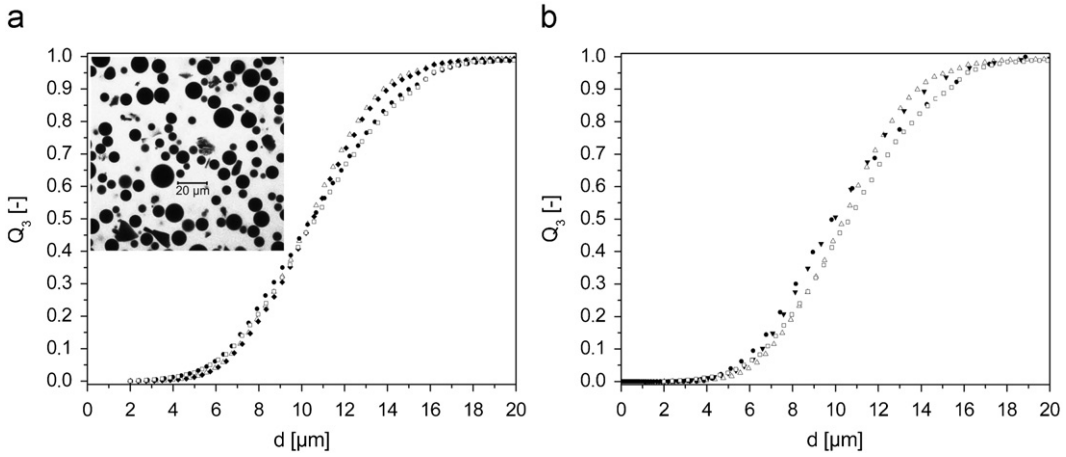

Fig. 4. CLSM images of glass particles dispersed in oil (field of view 142.9 μm × 142.9 μm) are analysed for quantification of both systematic errors. The slice error here has the dominant effect. (a) Original particle size distribution (△) and its corrections due to section (♦) and slice (●) errors and summed-up corrections (□). (b) Comparison of statistical analysis of CLSM images (without (Δ) and with both error corrections (□), laser diffraction (●) and Coulter counter measurement (▼). The agreement is satisfactorily when taking into account systematic and statistical errors of all three methods. For better illustration the number of data points was reduced by a factor of 25.

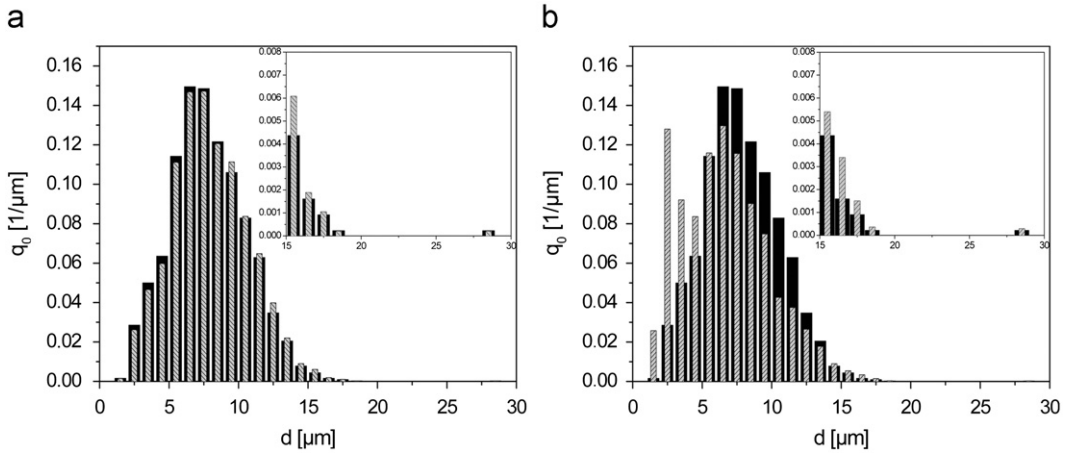

Fig. 5. The q_0 droplet size distribution changes due to the corrections: the influence of (a) the optical section error correction and (b) the slice error correction. The insets show a zoom of the range of larger droplet sizes. Corrections are hatched grey, the bars of the uncorrected distribution are filled black.

t is the Student-factor (Sommer, 1979). The relation between the discrete cumulative number related distribution Q_0 and the discrete cumulative volume related distribution Q_3 can be obtained via the density of the volume related distribution function:

$$Q_0(\bar{d}_n) = \frac{\sum_{i=1}^{n} \bar{d}_i^{-3} q_3(\bar{d}_i)(d_{i+1}-d_i)}{\sum_{k=1}^{N} \bar{d}_k^{-3} q_3(\bar{d}_k)(d_{k+1}-d_k)} \quad (4)$$

As Q_0 is generally not known, an empirical way for its determination is described in the following. It is clear, that the distribution's width is one parameter which has an influence onto the required number of analysed droplets. For methods, which use a classification scheme, also the class width has to be taken into account.

In a CLSM analysis shown here, the analysed number of droplets was varied while keeping the basic droplet population constant. The resulting volume related cumulative DSD Q_3 was calculated as a function of the number of analysed droplets (Fig. 6(a)). Q_3 approaches a limit for the increasing number of analysed droplets as expected. The normalisation of Q_3 or equivalently the integral normalisation of its density distribution q_3 causes the Q_3 value for the largest analysed droplet to be 1, which is in the present case a matter of the number of analysed droplets. The impression of larger possible values than 1 for the increasing number of analysed droplets is caused by this fact. For estimation of the minimum number of droplets required for a reliable DSD, the described approach was applied on five emulsions with different DSDs, leading to Fig. 6(b), which allows an estimate for the required number of analysed droplets n for a given span $B_N=(d_{90,3}-d_{10,3})/d_{50,3}$. Assume, that the relevant number of droplets n is asked for an emulsion with an expected span of 2. According to Fig. 6(b), n can be estimated to $n>9000$, for which the resulting DSD will reach its asymptotic values. Vice versa, the DSD of an analysed emulsion can subsequently be controlled in terms of the statistical accuracy (Fig. 6).

3.4. Application of CLSM to $W_1/O/W_2$ double emulsion

Most of the analytical scattering methods like laser diffraction, ultrasonic attenuation and dynamic light scattering are not well suited for the characterisation of double emulsions due to multiple scattering on inner droplets. NMR was shown to deliver the W_1 DSD with a sufficient accuracy under the assumption of a log-normal distribution function (Bernewitz et al., 2011). A CLSM analysis was performed on a $W_1/O/W_2$ emulsion, in which the oil phase was dyed by Nile Red. The CLSM images (Fig. 7, inset) show clearly that both, the inner water phase and the oil phases can be differentiated with a satisfying signal-to-noise ratio. Furthermore, the images show a statistically distributed W_1-phase in the oil phase, which again shows no clustering, but a broad distribution of sizes. Therefore, applying statistical methods, both, the inner and the outer DSD can be determined from one set of CLSM images (Fig. 7), keeping in mind that a sufficiently large number of droplets has to be considered: 15962 W_1 droplets entered the W_1-DSD. 2547 droplets are analysed for O, which is at the limit of statistical relevance. Statistical image processing of CLSM data sets is shown to be a valuable tool for getting insight into the size distributions of otherwise hardly describable structures. Good agreement of DSDs of W_1-droplets in $W_1/O/W_2$-double emulsions obtained by statistical image data processing of CLSM images as well as high- and low-field NMR has been shown (Bernewitz et al., 2011).

As only the oil phase is observed in this example, the question should be addressed whether air bubbles could influence the results, which would be important especially in cases of highly viscous intermediate phases. Despite of the fact that it is unlikely that large amounts of air bubbles in the interesting size range are permanently present in a double emulsion and despite of the good agreement with the W_1-DSD determined by NMR, the so far discussed CLSM procedure would not be able to differentiate between W_1 droplets and air bubbles. A solution to this problem would be the dying of the water phases with e.g. Fluorescein–Sodium (green fluorescence) and the dying of the oil phase e.g. with Nile red (red fluorescence). Acquiring a two channel image will lead to a positive image of water (green channel), which could be compared with the oil image (red channel) for air bubble identification.

CLSM, combined with statistical image analysis, is a well suited method for the determination of DSDs of both, the inner and the outer emulsion. As discussed in the introduction, the currently used instrumentation in emulsion characterisation (e.g. laser diffraction) is limited in this respect. The CLSM image analysis has therefore an important impact and large potential for the optimisation of processing parameters of the emulsification.

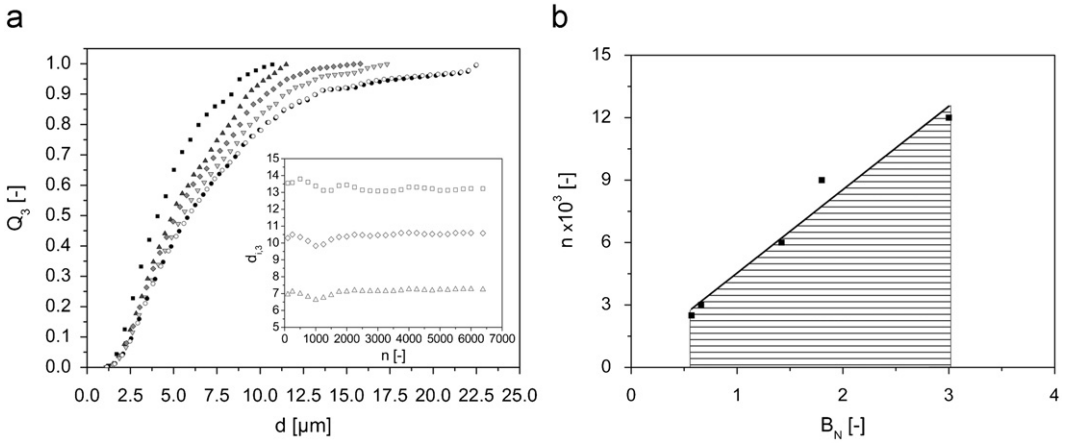

Fig. 6. Influence of the number of analysed objects n in statistical image analysis: (a) In the case of the W_1 DSD of a $W_1/O/W_2$ emulsion, Q_3 shows an asymptotic behaviour with $n \to \infty$. For illustration, the size of the data set was reduced by a factor of 15. The symbols are for the following values of the number n of analysed objects and the span B_N: n/B_N: ■ 2000/1.55; ▲ 4000/1.40; ♦ 6000/1.55; ◇ 8000/1.60; ● 9000/1.82; ○10000/1.80. In the inset, the determination of the critical number of droplets to be analysed is illustrated for the quantiles $d_{10,3}$ (Δ), $d_{50,3}$ (◇); $d_{90,3}$ (□): the characteristic numbers of the distribution converge for $n \to \infty$. (b) The statistically required number of droplets n and the span B_N are related: in the ruled range, n is too small for a statistically significant data processing, whereas above the line, the calculated DSD becomes meaningful.

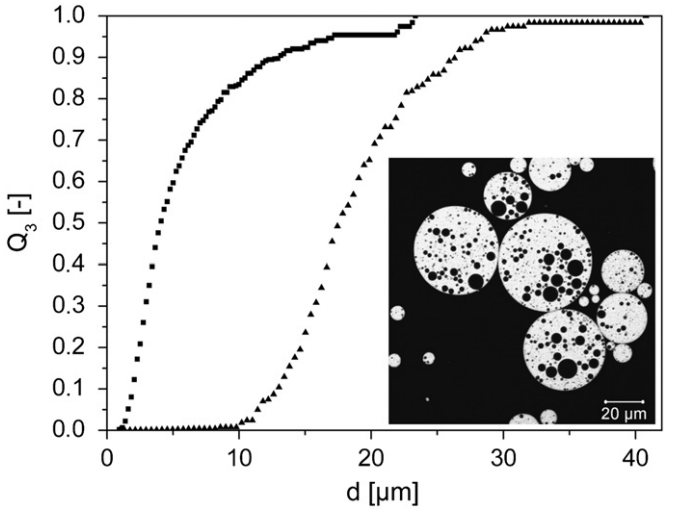

Fig. 7. Simultaneous determination of both, the inner (W_1, ■) and outer (O, ▲) cumulative DSDs of a double emulsion. The oil phase was dyed with Nile Red. The DSDs are statistically consistent. The inset shows the CLSM image of the $W_1/O/W_2$ with the oil phase dyed (field of view 142.9 µm × 142.9 µm).

In addition to the determination of DSDs of the inner and outer phases, it was noticed that dye diffuses between the water phases: CLSM images were recorded while the outer water phase was dyed. Within a few seconds, also the inner water droplets showed fluorescence, which can be explained only by diffusion of dye molecules between water phases through the oil phase. These findings are in agreement with the molecular exchange found in NMR experiments on double emulsions, where molecular water exchange could be observed and quantified (Guan et al., 2010; Hindmarsh et al., 2005; Mezzenga et al., 2004; Wolf et al., 2009).

4. Conclusions

CLSM gives detailed insights into complex structures like (double-) emulsions. The arrangement of droplets is revealed, in single as well as in double emulsions. The latter is of special interest as analysing these structures by conventional methods is extremely challenging. Moreover, CLSM combined with statistical image analysis yields DSDs, which are important quantities for characterising emulsion systems with respect to their mechanical and product properties as well as microbial stability. Systematic errors have to be considered, the DSDs are corrected statistically by their influence, namely the slice error and the optical section error. An empirical way is proposed for the estimation of the statistically relevant number of droplets which should be analysed for obtaining the limiting values of the DSD. The approach was proven for glass sphere suspensions and single emulsions. Furthermore, also double emulsions can be analysed with respect to the DSDs of both, the W_1 phase and the oil phase. By application of the CLSM approach, the inner and outer DSDs of a $W_1/O/W_2$ emulsion were determined simultaneously, which is currently unsurpassed by any other analytical technique. Additionally, questions like exchange between phases, coalescence and agglomeration could be answered by this imaging technique.

Acknowledgement

The "Shared Research Group 10-2" received financial support by the Concept for the future' of Karlsruhe Institute of Technology (KIT) within the framework of the German Excellence Initiative. The Fraunhofer Institute for Chemical Technology in Pfinztal-Berghausen is thanked for a very substantial financial support. The cooperation project of LVT and SRG10-2 was financially supported by the Deutsche Forschungsgemeinschaft (project SCHU 1417/4-1). The CLSM was kindly provided by Prof. Dr. M. Bastmeyer of the Zoological Institute, Department of Cell and Neurobiology in Karlsruhe, Germany within the frame of the KIT-Center for Functional Nanostructures CFN. Special thanks to Azad M. Emin for discussions and introduction to the CLSM method.

References

Benichou, A., Aserin, A., Garti, N., 2004. Double emulsions stabilized with hybrids of natural polymers for entrapment and slow release of active matters. Adv. Colloid Interface Sci. 108-109, 29–41.
Bernewitz, R., Guthausen, G., Schuchmann, H.P., 2011. NMR on emulsions: characterisation of liquid dispersed systems. Magn. Reson. Chem. 49, S93–S104.
Blonk, J.C.G., Vanaalst, H., 1993. Confocal scanning light-microscopy in food research. Food Res. Int. 26, 297–311.
Cruz-Orive, L.M., 1976. Particle size-shape distributions: the general spheroid problem, I mathematical model. J. Microsc. 107, 235–253.
Cruz-Orive, L.M., 1983. Distribution-free estimation of sphere size distributions from slabs showing overprojection and truncation, with a review of previous methods. J. Microsc. 131, 265–290.
Gegner, J., Henninger, C., Öchsner, A., 2004. Stereologic analysis and modelling of object distributions from sectional micrographs. Materialwiss. Werkstofftech. 35, 36–44.
Goldsmith, P.L., 1967. The calculation of true particle size distributions from the sizes observed in a thin slice. Br. J. Appl. Phys. 18, 813–830.
Guan, X.Z., Hailu, K., Guthausen, G., Wolf, F., Bernewitz, R., Schuchmann, H.P., 2010. PFG-NMR on W1/O/W2-emulsions: evidence for molecular exchange between water phases. Eur. J. Lipid Sci. Technol. 112, 828–837.
Hindmarsh, J.P., Su, J., Flanagan, J., Singh, H., 2005. PFG-NMR analysis of intercompartment exchange and inner droplet size distribution of WOW emulsions. Langmuir 21, 9076–9084.
Lamprecht, A., Schäfer, U., Lehr, C.M., 2000. Structural analysis of microparticles by confocal laser scanning microscopy. Pharm. Sci. Technol. 1.
Landfester, K., 2009. Miniemulsion polymerization and the structure of polymer and hybrid nanoparticles. Angew. Chem. Int. Ed. Engl. 48, 4488–4507.
Mao, S.R., Xu, J., Cai, C.F., Germershaus, O., Schaper, A., Kissel, T., 2007. Effect of WOW process parameters on morphology and burst release of FITC-dextran loaded PLGA microspheres. Int. J. Pharm. 334, 137–148.
McClements, D.J., Decker, E.A., Park, Y., Weiss, J., 2009. Structural design principles for delivery of bioactive components in nutraceuticals and functional foods. Crit. Rev. Food Sci. Nutr. 49.
Mezzenga, R., Folmer, B.M., Hughes, E., 2004. Design of double emulsions by osmotic pressure tailoring. Langmuir 20, 3574–3582.
Muschiolik, G., 2007. Multiple emulsions for food use. Curr. Opinion Colloid Interface Sci. 12, 213–220.
Pawley, J.B., 1995. Handbook of Biological Confocal Microscopy. Plenum Press.
Reverter, J.C., Feliu, E., Climent, C., Rozman, M., Berga, L., Rozman, C., 1993. Stereological study of human bone-marrow adipocytes—a comparison of 4 methods for estimating size distributions. Pathol. Res. Pract. 189, 1215–1220.
Skorobogat, L.I., Podobeda, L.G., 1975. Theory, production technology, and properties of powder and fibers, particle-size analysis of powders by the cord method. Poroshk. Metall. 11, 1–4.
Sommer, K., 1979. Probenahme von Pulvern und körnigen Massengütern: Grundlagen, Verfahren, Geräte. Springer-Verlag, Berlin.
Sommer, K., 1995. Randfehlerkorrektur bei der Bildanalyse von Partikeln. Chem. Ing. Tech. 67, 1638–1641.
van Dalen, G., 2002. Determination of the water droplet size distribution of fat spreads using confocal scanning laser microscopy. J. Microsc. 208, 116–133.
van Duynhoven, J.P.M., Goudappel, G.J.W., van Dalen, G., van Bruggen, P.C., Blonk, J.C.G., Eukelenboom, A.P.A.M., 2002. Scope of droplet size measurements in food emulsions by pulsed field gradient NMR at low field. Magn. Reson. Chem. 40, S51–S59.
Wicksell, S.D., 1925. The corpuscle problem: a mathematical study of a biometric problem. Biometrika 17, 84–99.
Wolf, F., Hecht, L., Schuchmann, H.P., Hardy, E.H., Guthausen, G., 2009. Preparation of W1/O/W2 emulsions and droplet size distribution measurements by pulsed-field gradient nuclear magnetic resonance (PFG-NMR) technique. Eur. J. Lipid Sci. Technol. 111, 723–729.